Precipitation Characteristics of Mesoscale Convective Weather Systems

R. J. KANE, JR.*, C. R. CHELIUS AND J. M. FRITSCH

Department of Meteorology, The Pennsylvania State University, University Park, PA 16802

(Manuscript received 19 January 1987, in final form 28 March 1987)

ABSTRACT

Precipitation from 74 mesoscale convective complexes is examined to determine the total precipitation, areal extent, and characteristic precipitation pattern of an average convective complex. The relationship between the average precipitation pattern and the track of the centroid of the satellite-observed, cold-cloud shield is determined as an aid to forecasting. The amount and spatial distribution of precipitation during each stage (i.e., initiation, maturation and dissipation) of the average convective system's life cycle are presented, as well as the precipitation patterns for systems that form in particular synoptic environments. The precipitation characteristics of MCCs are compared to those from 32 other convective weather systems that are similar to MCCs but do not meet all the MCC-definition criteria.

1. Introduction

It has been known for some time that convective precipitation exhibits a nocturnal maximum over the Central Plains of the United States with a progressive spatial diminution in all directions (Kincer, 1916). This maximum is probably related to the well-organized meso-α scale[1] convective weather systems that frequent this geographical region. Maddox (1980) termed the largest class of these convective systems Mesoscale Convective Complexes (MCCs). Studies of the annual frequency of MCCs over the Central Plains (Maddox, 1980; Maddox et al., 1982; Rodgers et al., 1983, 1985) indicate that MCCs are relatively common; typically 30 to 50 MCCs occur during each warm season (March–September). The fact that much of the deep convection in this region tends to occur in such an organized manner offers promise of significant improvements in warm-season quantitative precipitation forecasts (QPF) if the development and movement of these systems can be predicted. Therefore, many efforts to understand the structure and dynamics of these convective mesosystems have already been completed (e.g., Maddox et al., 1981; Fritsch and Brown, 1982; Wetzel et al., 1983; Maddox, 1983; Smull and Houze, 1985; Leary and Rappaport, 1987). Moreover, several studies of the precipitation characteristics of MCCs have now been completed. Specifically, Howard and Maddox (1983) showed that MCCs produce significant (>2.5 mm) precipitation over extensive geographical areas. Bosart and Sanders (1981) documented that convective complexes may exist for up to several days, but, because they undergo diurnal oscillatory growth and decay, their extensive precipitation tracks are sometimes intermittent. Nevertheless, Fritsch et al. (1986) found that MCCs account for 30–50% or more of the warm season rainfall over much of the region between the Rocky Mountains and the Mississippi River. McAnelly and Cotton (1986) examined the small-scale structure of MCC precipitation patterns and found that, although there is a uniform cold-cloud shield associated with MCCs, the precipitation distribution exhibits large variability. Most of the heavy precipitation coincides with meso-β scale areas of intense convective activity. Merritt and Fritsch (1984) and Bartels and Rockwood (1983) found a preferential development region for meso-β elements along the right (typically equatorward) flank of MCCs. This flank is normally the region of strongest convergence of the low-level inflow of conditionally unstable air (Maddox, 1983).

The aforementioned studies led to speculation that MCCs may routinely produce an asymmetrical but frequently similar precipitation pattern. Knowledge of such a routinely occurring asymmetrical precipitation pattern may be helpful for forecasting heavy precipitation during MCC passage. This is particularly true for hydrologists as well as meteorologists, since knowledge of extremes and averages of convective mesosystem precipitation is important in flood control, structure durability, soil moisture budgets and water resource management. It is likely that the agricultural community would also be interested in the precipitation characteristics of MCCs, since these convective mesosystems distribute widespread beneficial rainfall

* Present affiliation: National Weather Service Office, Greensboro, NC 27419-0146.

[1] Meso-α scale: length scales of 250–2500 km and duration of $\geq$6 h; meso-β scale: length scales of 25–250 km and duration of <6 h. (See Orlanski, 1975.)

throughout the central United States at a critical time in the growing season.

The primary purpose of this investigation is to determine the average temporal and spatial characteristics of precipitation from mesoscale convective weather systems and to develop a relationship between the average precipitation pattern and the satellite-observed cold-cloud shield.

2. Data

Maddox et al. (1982) noted that there are many convective mesosystems that lack either the duration, shape or size necessary to be considered MCCs. Moreover, routine examination of satellite imagery and conventional meteorological data suggests that there is an entire spectrum of MCC and MCC-type systems in which the thermodynamic and dynamic mechanisms during their development, propagation, maturation and dissipation are similar. Those MCC-type or MCC-like events, which for various reasons such as size or duration, do not meet the MCC criteria established by Maddox (1980), but nevertheless manifest many of the characteristics of MCCs, will be termed Mesoscale Convective Systems (MCSs). Specifically, each MCS meets Maddox's eccentricity (shape) requirement, has a $-32°C$ cold-cloud shield of at least 6×10^4 km^2, and persists at this size or greater for at least 4 h. [See Fritsch et al. (1986) for further discussion of the MCS selection criteria.]

For the purposes of this paper, the entire MCC/MCS dataset will be termed Mesoscale Convective Weather Systems (MCWS). The dataset includes 106 events that occurred in the United States from March–September 1982 and 1983. All of the MCCs and almost all of the major MCSs for the 2 years are included; a total of 74 MCCs and 32 MCSs were included in the study (see Table 1). Several apparent MCS events were excluded because of incomplete satellite and/or precipitation data.

The two primary sources of precipitation data are 24-h precipitation charts obtained from the Heavy Precipitation Branch (HPB) at the National Meteorological Center (NMC), and hourly precipitation reports from the National Climatic Data Center. On some occasions these data are supplemented with 24-h daily rainfall amounts available from the standard NMC facsimile charts and with hourly amounts from surface station observations. The 24-h precipitation charts from HPB are produced from a network of over 7000 stations stretching from the East Coast to the Rockies. This is an extremely large number of precipitation-reporting stations, particularly when compared to the approximately 700 hourly observing stations located throughout the same area. For example, the state of Iowa contains a potential reporting density of approximately 254 stations versus the hourly precipitation data of only 68 stations. However, because of its temporal resolution, the hourly precipitation data is crucial in delineating many precipitation patterns. Consequently, in most cases a combination of the two data sources is used to attain the highest degree of accuracy and the best temporal resolution possible for a particular event.

TABLE 1. Frequency of MCCs, MCSs and MCWSs for 1982 and 1983.

	Number of events		
Year	MCCs	MCSs	MCWSs
1982	44	16	60
1983	30	16	46
1982–1983	74	32	106

3. Methodology

An "event-oriented" approach is employed, wherein each accumulated-precipitation pattern has boundaries defined by the entire lifetime of an individual convective complex or system. This type of an approach provides a continuous accumulated precipitation swath for each system, starting from the genesis period (time of first storms) to dissipation. However, this approach also resulted in a number of analysis problems. For example, sometimes one convective mesosystem spawned another system and it became difficult to separate the two systems. In this case, the first system was terminated and a new one initiated when the cold-cloud shield again started to expand. Often a system originated from several "first-storm complexes" that developed over different parts of a state, combined, and finally formed a mature complex. The rainfall produced by *all* of the original storms was incorporated into the final precipitation field. In several instances convective mesosystems split in two (e.g., see McCann, 1983). One system would remain quasi-stationary, while the other propagated eastward, or the individual systems would propagate in different directions. In either case, upon splitting, a separate precipitation field is determined for each system. The precipitation common to each system is considered as if each system occurred independently from the other.

The primary technique to determine the precipitation characteristics of the average system consists of the following steps:

(i) The time and space domains of the precipitation from each system are determined from radar, satellite and conventional observations. If all the precipitation that occurred in the time and space domains of a particular system was the result of that system, then the 24-h reporting station data are used directly to establish the rainfall pattern. If overlapping events occurred, or if precipitation occurred in the convective mesosystem domain as a result of other processes, e.g., from a cold front, then the hourly precipitation data are used to

estimate (by linear interpolation) the fraction of the total rainfall that was produced by the convective mesosystem at each 24-h reporting station.

(ii) The resulting precipitation field from step (i) is analyzed using the Penn State analysis system (Cahir et al., 1981). The analysis produces an evenly spaced network of grid point values 50 km apart.

(iii) The total grid point rainfall (P_k) and the average rain depth ($\bar{P}_k$) over the storm area are calculated for each event (k) and for certain groups of events. The total rainfall is obtained from

$$P_k = \sum_{i,j=1}^{i,j=I,J} p_{i,j}, \tag{1}$$

where I and J are the maximum grid point indices defining the domain and $p_{i,j}$ is the precipitation at the grid point with indices i, j. The average rain for a particular event is then

$$\bar{P}_k = \frac{P_k}{N_k}, \tag{2}$$

where N_k is the number of nonzero grid elements in the domain of the kth event.

(iv) The mean precipitation for various subsets or groups of MCC or MCS events are computed. It is sometimes desirable to determine the mean precipitation for various groups of MCWSs that occur under similar meteorological conditions or over the same geographical region. To find the mean precipitation ($\bar{P}_G$) for a group of events, there is an important area/depth relationship that must be considered. For example, two events may produce the same $\bar{P}$ but one storm may have distributed rainfall over a larger area. Hence, the mean precipitation for each event must be area-weighted. The group mean is therefore defined by

$$\bar{P}_G = \frac{\sum^{K} (A_k)(\bar{P}_k)}{\sum^{K} (A_k)}, \tag{3}$$

where K represents the set of k events included in the group and A_k is the total precipitation area of the kth event. The area A_k is defined by

$$A_k = N_k(\Delta x)^2, \tag{4}$$

where Δx is the mesh size (50 km).

(v) The average precipitation patterns for all MCWSs and for particular classifications or groups of MCWSs are computed. This is accomplished by compositing the objectively analyzed precipitation fields in each group or classification of events. Since the size and orientation of each precipitation field differ from one case to the next, compositing may smooth out the "characteristic pattern" or routinely occurring asymmetries that are being sought. Therefore, all of the precipitation fields are adjusted to a single size, hereafter referred to as the standard size, before compositing. Each precipitation pattern is also aligned with the axis of propagation of the convective system. Merritt and Fritsch (1984) found that convective mesosystems tend to propagate with the thermal wind vector (wind shear) in the cloud layer. Consequently, the axis of propagation for each particular pattern is defined to run approximately parallel to the thermal wind vector and intersect the centroid[2] of the precipitation pattern. In each case the precipitation pattern is rotated before compositing so that the thermal wind vector (or the axis of propagation) coincides with the x-axis (points in a heading of 90°). In this way all the systems are aligned as if they propagated in the same direction.

In adjusting the patterns to the standard size, each grid matrix is numerically expanded; i.e., using polar coordinates, each grid point is moved radially outward from the centroid of the precipitation field. Expansion is used rather than contraction because some data could possibly be lost or maxima reduced in the contraction of data toward a single center point. Consequently, to obtain the standard size, all matrices are expanded to the area of the largest storm. The amount of expansion (E) is calculated from the following expression:

$$E = \frac{(A_m/N_k)^{1/2}}{\Delta x}, \tag{5}$$

where m is the index of the largest event. Clearly, for $N_k = N_m$, $E = 1$. Therefore, the E value for the largest storm is 1, which is expected, and all other matrices will have an E value greater than 1. In this study, the E values ranged from 1 to 3.3; i.e., the largest system is about three times as large as the smallest system.

After the expansion procedure is completed, the precipitation arrays are rotated either clockwise or counterclockwise (depending upon the angle needed to bring the thermal wind vector and the x-axis into coincidence) around the centroid of the precipitation field. Since the expansion and rotation result in new locations for the original grid points, the "new" data points are objectively analyzed to determine the precipitation values at grid points within the standard size grid matrix. Figure 1 shows an example of an original precipitation field and the result after the size and rotational adjustments. When the values of the initial matrix are plotted against the values of the final matrix, a correlation of 0.985 results. Thus, the internal structure of the final pattern is very closely representative of the initial pattern. [See Kane (1985) for more details of the adjustment procedures.]

In addition to adjusting the precipitation arrays, the locations of the −32°C and −52°C centroids of the cold-cloud shield at the various MCC stages (initiation,

[2] Centroid is defined as the geometric center of the precipitation field, or that point in the center of the field at which symmetry is achieved.

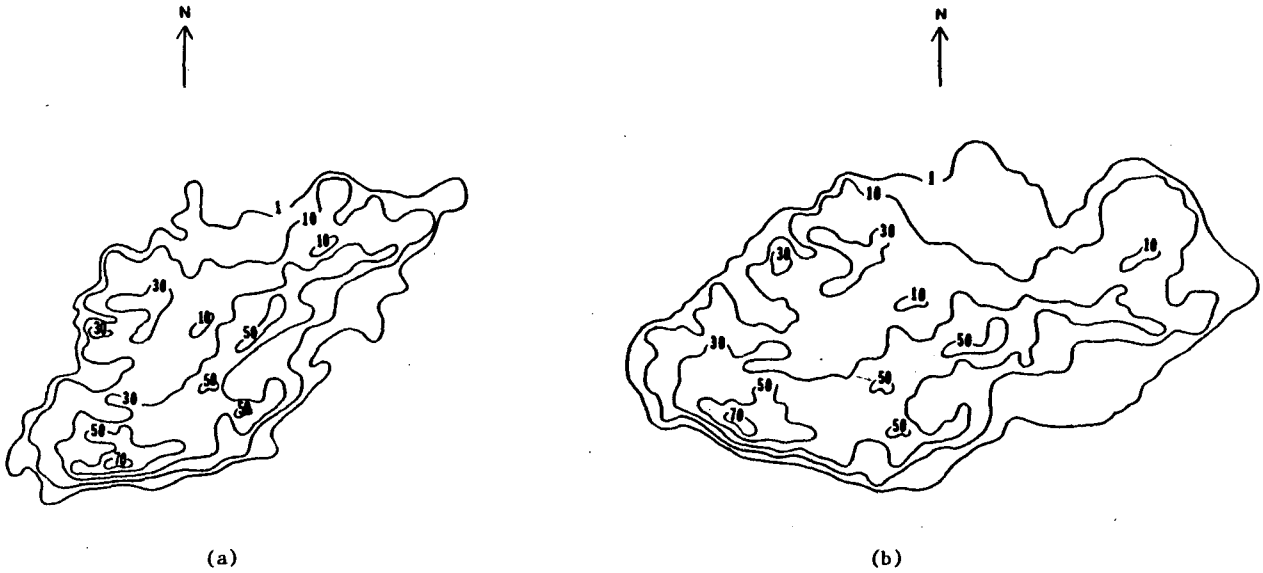

FIG. 1. (a) Original precipitation (millimeters) pattern; (b) final precipitation pattern after adjustment to the standard size, rotation and objective analyses have been performed.

maturation, etc; see Maddox, 1980) are also determined for each event. This is done by shifting the centroid locations outward and rotating them by the same amount as the grid points are shifted and rotated. The new centroid locations can then be composited along with the adjusted precipitation fields. In this manner, the mean path of the cold-cloud shield can be estimated by the best-fit curve through the locus of centroid points for all the stages in the life cycle of the convective systems. The average locations of the centroids for each stage help to reveal the temporal characteristics of the rainfall from the convective systems, and the mean path gives some indication how the rainfall is distributed with respect to the satellite-observed cold-cloud shield.

Finally, it is important to note that the adjusted arrays are only used in the analysis of precipitation patterns. Other characteristics of the precipitation fields (e.g., mean size, maximum precipitation, etc.) are all computed from the unadjusted arrays.

4. Results

a. Average MCC rainfall characteristics

The average MCC produces at least 1 mm of rain over approximately 500 000 km^2. The average rainfall over this area is about 16 mm and the composite maximum is 38 mm. The average heading of the attendant cold-cloud shield is 106°. Figure 2 shows that most of the heavy precipitation occurs in the first half of the storm's life cycle, or, more specifically, between MCC initiation and maturation. The fact that the heaviest precipitation is usually produced rather close to the midlife of the storm agrees with results of Pani and Haragan (1981). The −32°C average cold-cloud shield centroid track does not correlate well with the path of the heaviest precipitation. The −52°C cold-cloud shield centroid track, however, is more accurate in depicting these regions. Also, the southern half of the pattern exhibits a larger precipitation gradient and, most importantly, quadrant III appears to be the most critical quadrant followed by quadrant IV, as far as heavy precipitation is concerned. In particular, Table 2 shows the percent probability and areal coverage of various rainfall amounts for the total storm area and for each quadrant. The probability is the percentage of the total number of events that produced the designated amount of rainfall, and the areal coverage is the average area of those events which *did* produce the designated rainfall amount. Note that *every* MCC produced ≥26 mm of rain and that the average area of ≥26 mm is over 100 000 km^2. Note also that virtually all of the events produced ≥26 mm in quadrant III and that this quadrant alone accounted for over half of the heavy rain (>25 mm) area.

The passage of an MCC almost guarantees measurable rainfall over a broad area. For example, Fig. 3a shows the percent frequency for ≥1 mm of rainfall. The 100% probability isopleth encompasses an area of nearly 50 000 km^2. Moreover, the 50% isopleth encloses almost 500 000 km^2, an area nearly as large as the combined states of Illinois and Indiana. It is also noteworthy that the −52°C track bisects the region covered by the 100% isopleth. This indicates that although this centroid track (−52°C) may at times be displaced slightly to the north of the heaviest precipitation region, on the average, it virtually always describes an area in which some precipitation is occurring

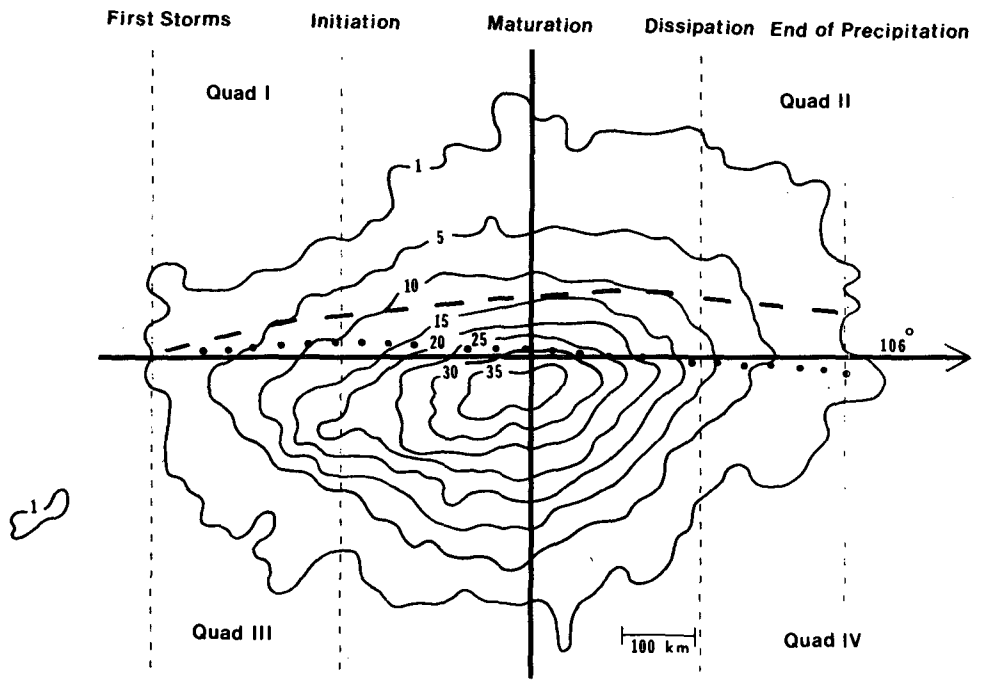

FIG. 2. Normalized composite precipitation (millimeters) pattern for 74 MCCs. The dashed and dotted lines are the approximate average centroid tracks of the −32°C and −52°C cold-cloud shields, respectively. The horizontal axis is the axis of propagation and indicates the average storm heading. Vertical dashed lines indicate approximate locations of various stages in the life cycle of the MCCs.

from just after MCC initiation to midway between MCC maturation and dissipation.

Figure 3b shows the percent frequency of ≥77 mm (3 in.) of rain. It is readily apparent that even for these large convective systems, it is rare for the same relative location to receive rain in excess of 77 mm. On the other hand, 77 mm of rain does not represent the highest maximum nor even the average maximum produced by the 74 systems. Table 3 is a compilation of statistics for the maxima produced by the 74 MCCs. Note that MCCs commonly produce a maximum of 75 mm or more.

TABLE 2. Probability and average areal coverage of various rain depths (mm) for all MCC events. Values are given for each quadrant and for all quadrants combined (total storm). Upper number is probability (%) and lower number is average area (10^3 km^2).

	Rain depth (mm)		
Location	≥26	≥51	≥77
Quad I	76 / 18.0	37 / 6.0	11 / 4.7
Quad II	72 / 20.8	34 / 5.9	8 / 3.3
Quad III	96 / 58.1	85 / 23.7	58 / 12.2
Quad IV	93 / 30.8	62 / 11.4	23 / 10.4
Total storm	100 / 112.0	93 / 34.1	66 / 15.6

Other important characteristics of MCC rainfall are evident from the statistics on the areal extent of the precipitation. Figure 4 shows the frequency distribution of the area of at least 1 mm of rain for the 74 MCCs. The average area covered, as mentioned previously, is approximately 500 000 km^2 while the median equals 430 000 km^2. The most frequently occurring size of the MCC precipitation area tends to be 250–350 × 10^3 km^2 with a secondary peak around 700 × 10^3 km^2. The range between the areal coverage of the largest and smallest MCC is 1 027 500 km^2. Obviously, there can be a tremendous difference in the precipitation distribution characteristics of MCCs.

b. Precipitation characteristics of subsets of MCCs

Since there are several different synoptic situations that lead to the formation of MCCs, it is possible that the precipitation characteristics may be significantly different for different types of large-scale environments. In order to explore this possibility, the MCC events were stratified into four categories: frontal, synoptic, mesohigh and extreme-right-moving (XRM) events. The synoptic conditions for the first three categories

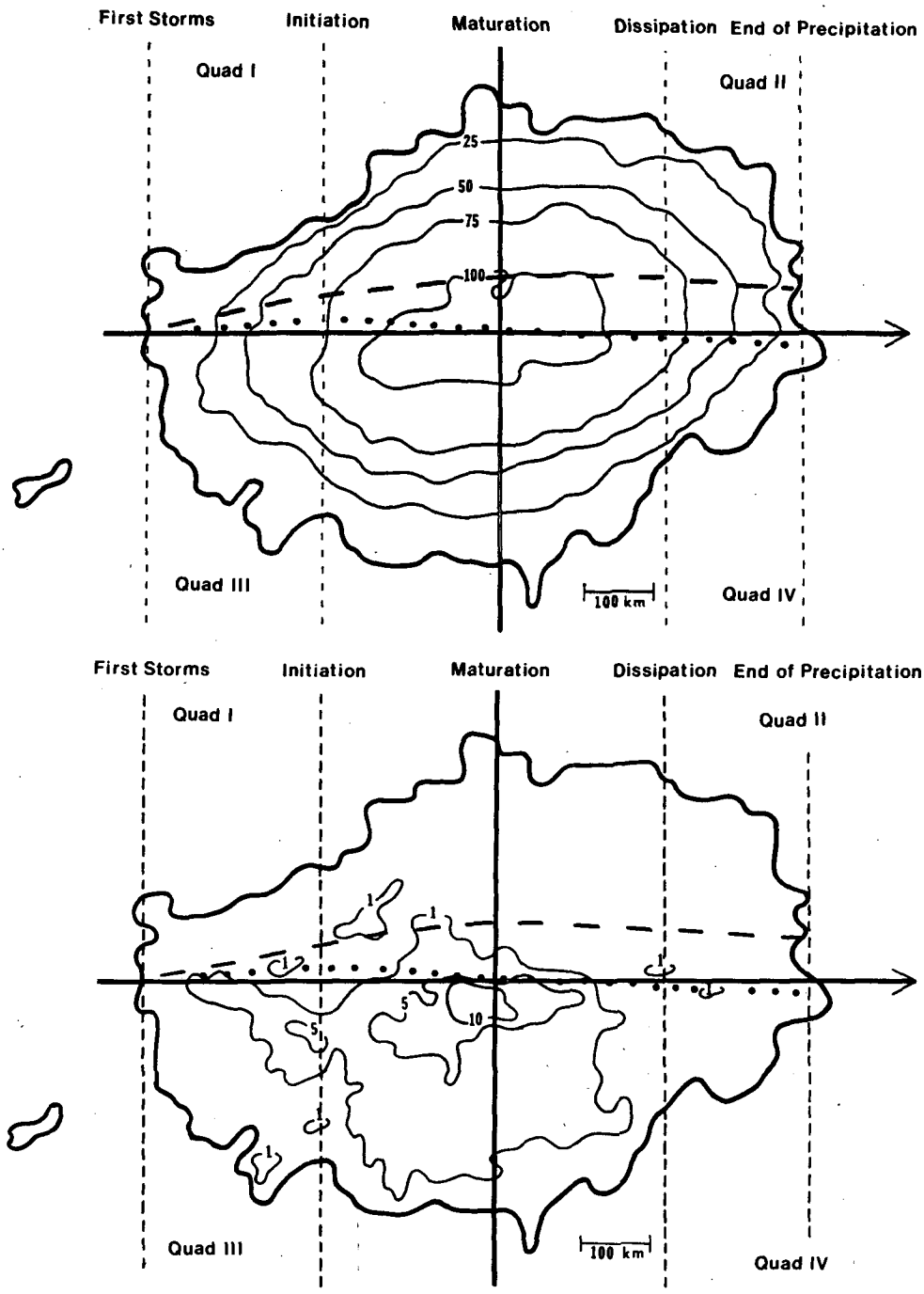

FIG. 3. Spatial distribution of (a) percent frequency ≥1 mm, (b) percent frequency of ≥77 mm for 74 MCCs. The outer isopleth is that of the 1 mm isohyet from Fig. 2. The remainder of the figure is as in Fig. 2.

were described by Maddox et al. (1979). The last category is actually a subset of the frontal category, but is treated separately because of the distinctive movement of the MCCs. The classification of each event was done by Merritt (1985), who investigated the movement of 100 MCCs. Based on Merritt's study and Maddox's (1979) synoptic description, Figs. 5a and b show typical locations and movements for the various classifications of MCCs. The mesohigh events are most often found in the warm sector detached from strong baroclinic zones. However, sometimes they originate in the proximity of a frontal boundary and then propagate into

TABLE 3. Characteristics of MCC precipitation maxima (mm).

Statistic	Precipitation max (mm)
Average	104
Median	89
Mode	75
Range	271
[extremes	296, 25]

the warm sector. Normally they are embedded in a rather weak pressure gradient and are often initiated by an outflow boundary from some previous system. These events also are often associated with a weak short-wave trough aloft and typically are positioned just to the west of the 500-mb long-wave ridge axis. Frontal events are also found just to the west of the 500-mb long-wave ridge axis. However they are, by definition, associated with a baroclinic zone. They form to the north or cool side of either a warm front or an east–west-oriented stationary front. Apparently, the front is the forcing mechanism that acts to initiate and help focus the convection. Synoptic events are usually found on the warm side of a slow-moving or quasi-stationary cold front in advance of a long (synoptic-scale) wave aloft. They can extend well into the warm sector and often exhibit rather strong diffluence at the 300 mb to 200 mb level.

Tables 4 and 5 and Fig. 6 present the results of stratifying the precipitation into the MCC categories. (The composite pattern for XRM events is not shown because of the small sample size.) It is evident that there is little difference in the precipitation patterns. As with the composite of all the MCCs, the heaviest rainfall for each of the categories occurs in quadrant III and the −52°C centroid track roughly bisects the precipitation fields. On the other hand, the rainfall area and amounts vary considerably. In particular, synoptic events produce almost double the rainfall area of mesohigh events and more than double the volume of water (Table 4). Rain production by frontal events is about midway between mesohigh and synoptic events. Notice that synoptic events tend to occur early in the warm season when forcing from large-scale dynamics is still relatively strong. On the other hand, mesohigh and extreme-right-moving events occur in mid- to late summer when

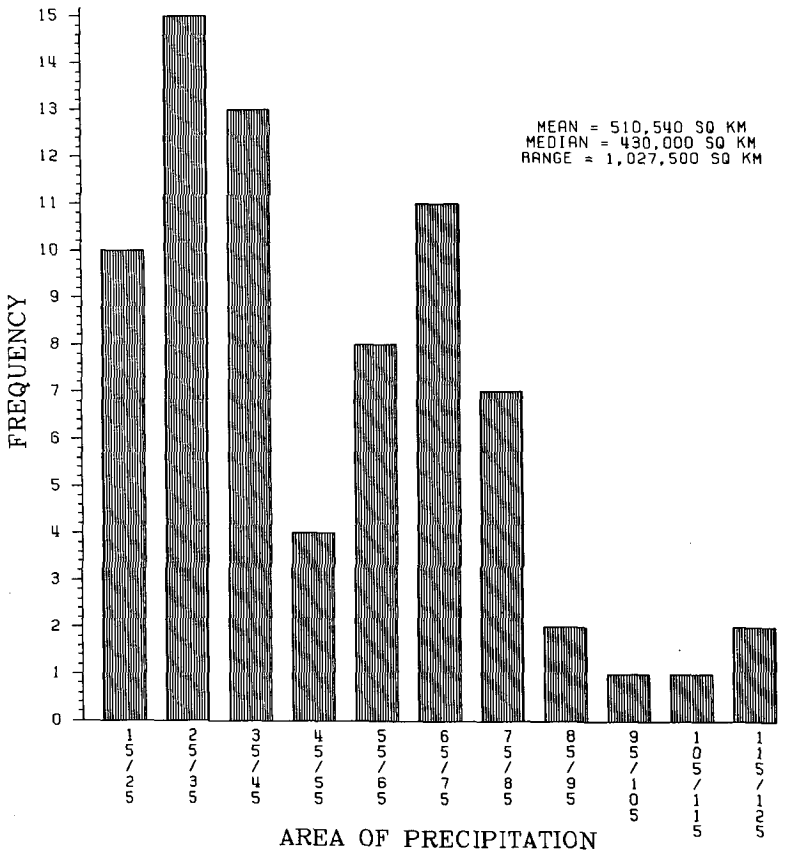

FIG. 4. Frequency distribution of the area of MCC precipitation. Vertical axis indicates the frequency of events and the horizontal axis indicates the area (times 10 000 km^2) covered by at least 1 mm of precipitation.

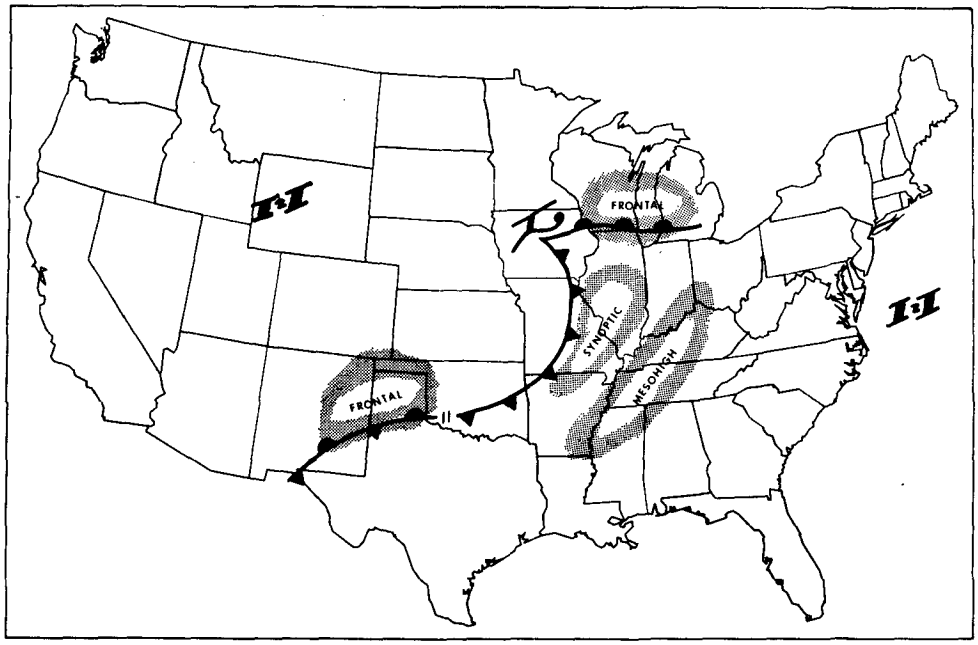

FIG. 5a. Generalized synoptic surface pattern indicating typical locations of the three main MCC classifications.

large-scale forcing is much weaker. Notice also that all systems in all categories produced over 26 mm of rain (Table 5). Additional stratifications of MCC precipitation (e.g., as a function of speed, longitude, low-level moisture, etc.) are described in Kane (1985).

c. *Comparison of MCC and MCS rainfall*

Figure 7 is the composite pattern of 32 MCSs from 1982 and 1983. Table 6 summarizes the precipitation characteristics for MCCs, MCSs and MCWSs for the

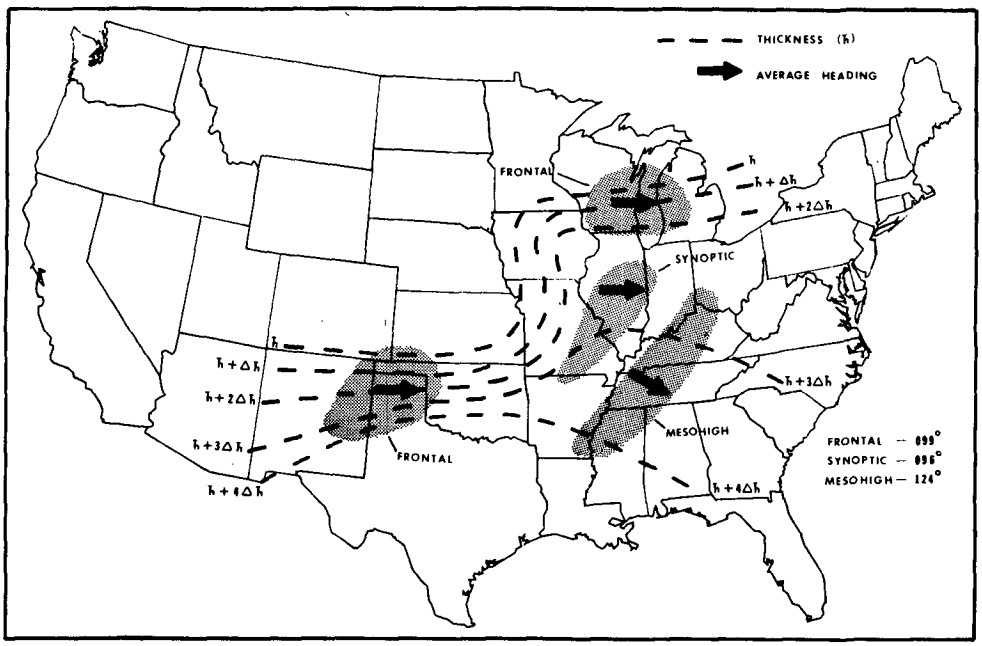

FIG. 5b. Approximate 850–300-mb thickness pattern associated with the generalized synoptic conditions of Fig. 5a. Dashed lines are the thickness contours and the arrows indicate headings of the convective systems.

TABLE 4. Precipitation characteristics of mesohigh, frontal, synoptic and extreme-right-moving MCCs.

Type of event	Number of events	$\bar{P}_G$ (mm)	Average maximum (mm)	Average area of ≥1 mm (10^3 km^2)	Average area of ≥26 mm (10^3 km^2)	Monthly distribution
Synoptic	20	17.9	129	678	167	Mar.—0 Apr.—6 May—5 June—5 July—3 Aug.—1 Sept.—0
Mesohigh	18	15.6	96	365	66	Mar.—0 Apr.—0 May—1 June—4 July—5 Aug.—6 Sept.—2
Frontal	32	15.1	96	505	107	Mar.—2 Apr.—2 May—7 June—9 July—4 Aug.—6 Sept.—2
XRM	4	14.5	79	408	87	Mar.—0 Apr.—0 May—0 June—2 July—1 Aug.—1 Sept.—0

same period. It is apparent that except for the size of the rain area, there is no significant difference between the rainfall characteristics of MCCs and MCSs (cf. Figs. 2 and 7). The lack of any significant differences in the composite precipitation characteristics or in the time of cold-cloud shield maximum extent strongly suggests that the dynamic and thermodynamic processes involved in MCCs and MCSs may be similar. With regard

TABLE 5. As in Table 2 except for mesohigh, frontal, synoptic and extreme-right-moving events. Frequency of each type are open in parentheses.

	Rain depth (mm)										
	Mesohigh (18)			Frontal (32)			Synoptic (20)			XRM (4)	
Location	≥26	≥51	≥77	≥26	≥51	≥77	≥26	≥51	≥77	≥26	≥51
Quad I	50 15.3	33 5.0	11 2.5	81 16.4	34 6.1	13 6.3	85 22.2	45 6.7	10 3.8	100 16.9	25 5.0
Quad II	61 10.9	39 3.5	6 2.5	72 20.2	34 5.2	6 2.5	85 28.1	35 7.9	10 5.0	75 18.3	50 3.8
Quad III	100 36.5	72 17.3	44 8.4	97 56.6	84 18.0	63 9.4	100 85.6	100 34.9	75 17.2	100 21.3	50 5.0
Quad IV	83 20.7	44 15.3	17 21.7	88 27.2	59 11.2	22 7.5	90 42.5	75 36.5	35 8.9	100 35.0	75 5.8
Total storm	100 65.8	89 24.8	56[3] 14.3	100 106.9	91 28.5	69 12.4	100 166.8	100 50.6	80 21.4	100 86.9	75 14.2

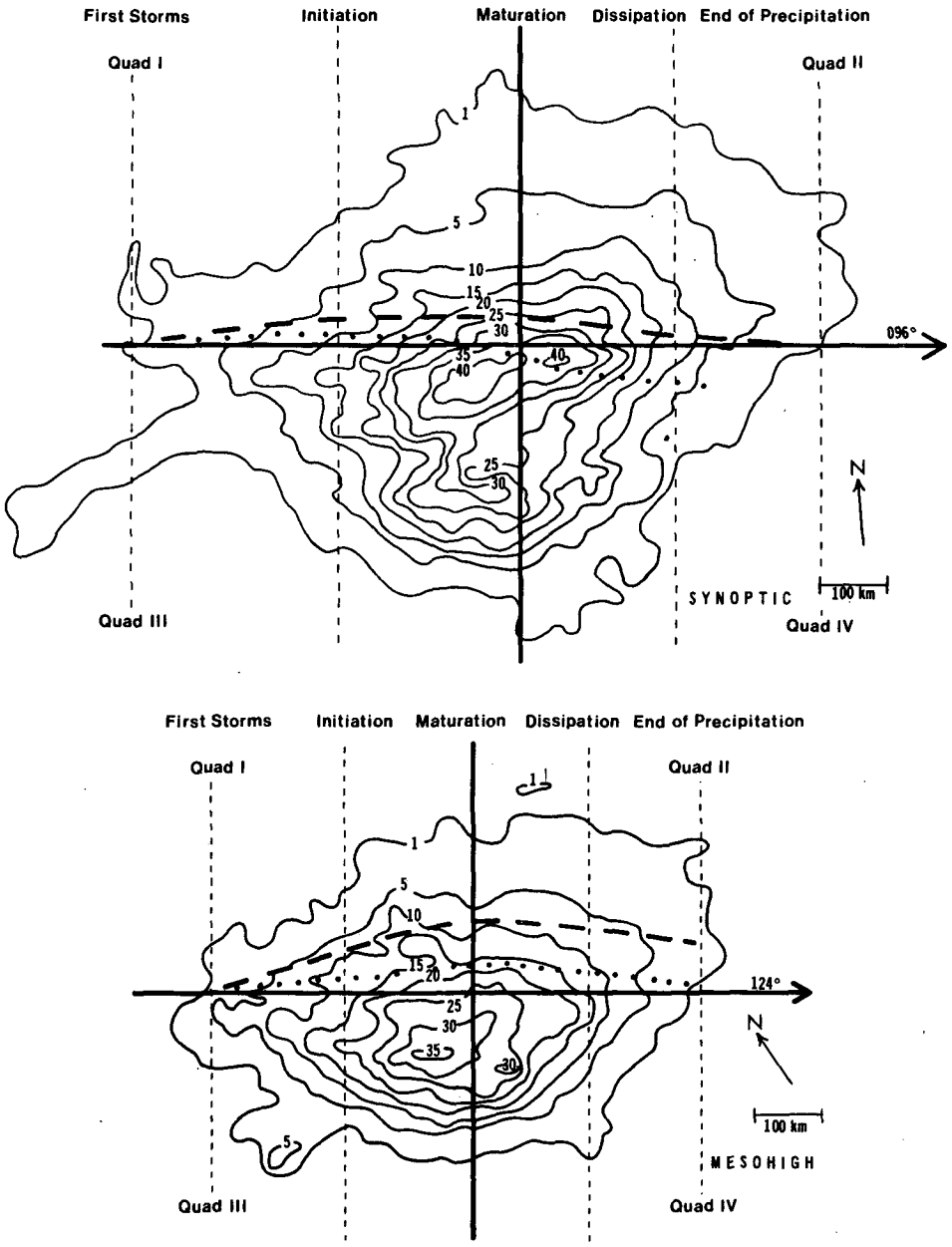

FIG. 6. As in Fig. 2, except for (a) 20 synoptic events, (b) 18 mesohigh events and (c) 32 frontal events.

to the large difference in size, it is interesting to note that most of the MCS events occurred in July and August, which is the same period when the relatively small mesohigh MCCs occurred. In fact, virtually all of the MCS events were mesohigh and frontal types, while in the MCC sample about one-fourth of the events were the heavy-rain-producing synoptic events.

5. Summary and concluding remarks

Based upon the rainfall from 74 MCCs, the "typical" MCC generates an average rain depth of 16.1 mm over 510 000 km^2. Undoubtedly, many MCC precipitation patterns rival the stratiform precipitation shields produced by extratropical cyclones. With respect to the direction of movement of the systems, the right-rear quadrant followed by the right-front quadrant are the regions of the precipitation pattern most frequented by heavy rainfall. These quadrants also represent that flank of the system most directly exposed to the low-level warm, moist inflow. Heavy precipitation can be produced in other sections of the precipitation pattern, although less frequently. Temporally, heavy rainfall usually appears from slightly after MCC initiation to

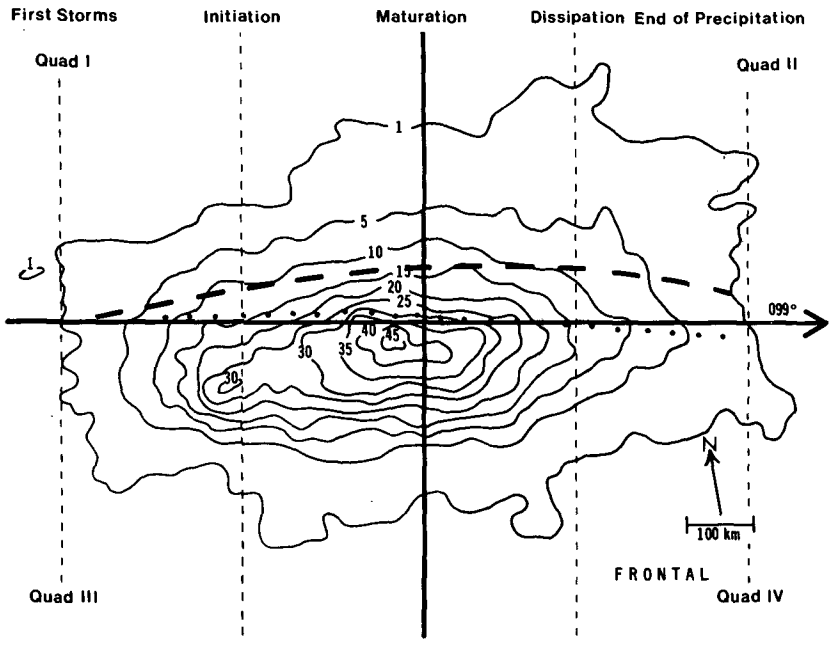

FIG. 6. (*Continued*)

slightly after MCC maturation. It is rare to have precipitation of ≥51 mm produced prior to MCC initiation or after MCC dissipation.

The track of the −32°C cold-cloud shield centroid does not correlate well with the center of the rainfall areas, however; the −52°C cold-cloud shield centroid provides a better correlation. In particular, the −52°C centroid track tends to bisect the rainfall area. Moreover, it does it in such a manner that the heaviest rainfall is usually slightly to the right of the path of the

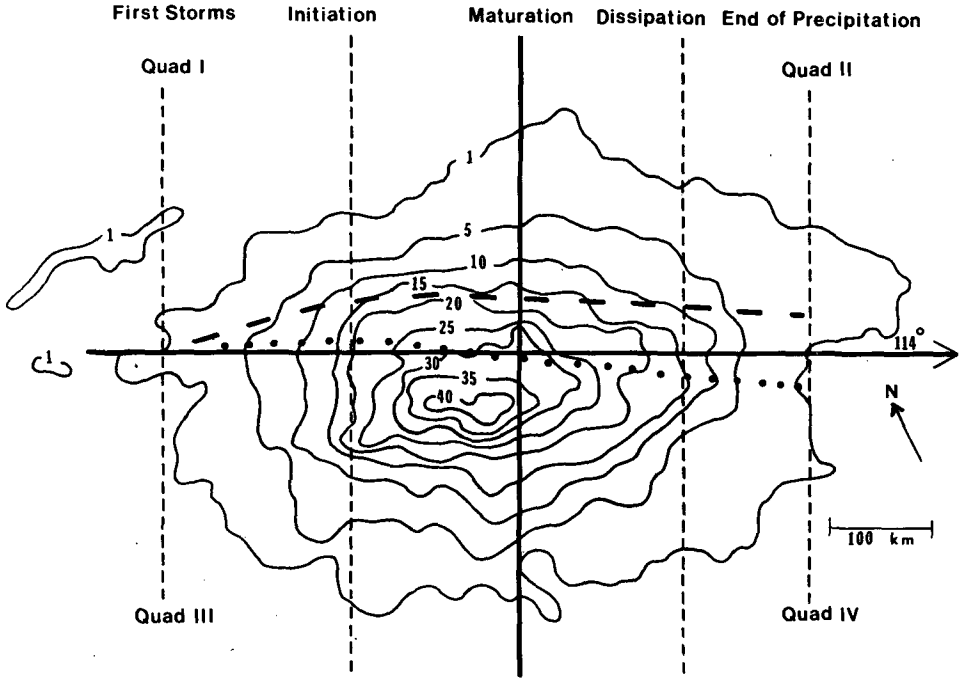

FIG. 7. As in Fig. 2, except for 32 MCSs.

TABLE 6. Precipitation characteristics of MCCs, MCSs, and MCWSs.

Type of events	Number of events	$\bar{P}_G$ (mm)	Average maximum (mm)	Average area of ≥1 mm (10^3 km^2)	Average area of ≥26 mm (10^3 km^2)	Monthly distribution	Average time of cold-cloud shield maximum extent (UTC)	Classification distribution
MCCs 1982 and 1983	74	16.1	104	511	112	Mar.—2 Apr.—8 May—13 June—20 July—13 Aug.—14 Sept.—4	0843	Mesohigh—18 Frontal—32 Synoptic—20 XRM—4
MCSs 1982 and 1983	32	16.2	98	285	64	Mar.—0 Apr.—0 May—4 June—5 July—10 Aug.—10 Sept.—3	0726 (31)*	Mesohigh—14 Frontal—16 Synoptic—2 XRM—0
MCWSs (total) 1982 and 1983	106	16.1	102	442	96	Mar.—2 Apr.—8 May—17 June—25 July—23 Aug.—24 Sept.—7	0820 (105)*	Mesohigh—32 Frontal—48 Synoptic—22 XRM—4

* Shows number of cases used in the calculation because of unavailable data.

centroid. Knowledge of this relationship may be helpful for short-term forecasting.

The MCC events were stratified into four categories that reflect different synoptic environments: frontal, mesohigh, synoptic and extreme-right-moving. Precipitation from each category of MCC was composited. There were no significant differences in the rainfall patterns of the various classifications. However, the size of the rain area and the magnitude of the rainfall amounts varied considerably. In particular, synoptic events produced about twice as much rain, in both area and volume, as mesohigh events. Since synoptic events tended to occur early in the warm season (April–May–June) while mesohigh events developed most frequently in July and August, the difference in rainfall area and magnitude may reflect a general weakening of the large scale dynamics from late spring to late summer. This implies that in mid- to late summer, the size of the rain area may be more dependent upon the latent heat release and internal dynamics of the convective system than in the spring.

The precipitation from 32 mesoscale convective systems (MCSs) was examined and compared to that from the 74 MCCs. The mesoscale convective systems were very similar to MCCs but for one reason or another (such as insufficient size or duration) did not meet all the MCC criteria. Except for size of the rain area, there were no significant differences between the MCC and MCS precipitation characteristics. The average MCC rainfall area was nearly 80% greater than the MCS area; however, the average maximum and the average rainfall per unit area were about the same. The precipitation patterns were very similar and the average time of maximum cold-cloud shield extent was nearly the same. This suggests that the dynamic and thermodynamic processes involved in MCC and MCS formation and maintenance may be essentially the same. In this regard, it is interesting that, as with mesohigh MCC events, most of the MCS events occurred in July and August when forcing from large-scale dynamics is generally weaker than in the spring. Therefore, it is possible that the smaller midsummer systems are more representative of the results of the forcing from the *convective* heating and moistening than the springtime events where large-scale processes can overwhelm and obscure the effects of the deep convection.

Finally, from information provided in this study, forecasters faced with MCC or MCS passage can recognize the particular zones and temporal margins of the oncoming cold-cloud shield that are most likely to produce heavy precipitation. In addition, it is possible to roughly estimate other precipitation characteristics such as the mean, extremes, areal coverage, etc. From the forecasters standpoint, though, it is extremely important to realize that the mean patterns of net precipitation from MCCs and MCSs probably do not resemble the rainfall rate patterns at any instant during the life of any given system. In particular, in some cases the maximum precipitation rates occur at the leading edge of the system during virtually its entire lifetime

(e.g., see Leary and Rappaport, 1987). On the other hand, the heaviest precipitation rates persist along the back edges of other systems (e.g., Hoxit et al., 1978). The precipitation patterns derived in the present study are more appropriate for forecasting the total precipitation and its spatial distribution during passage of an entire MCC or MCS.

Acknowledgments. The authors express their gratitude to Dr. Fregory Forbes for his critical review of this manuscript and to Jonathan H. Merritt for sharing the results of his work and for his help and input on many aspects of the investigation; to David A. Olson of the National Meteorological Center, Howard Edwards of the National Climatic Center and Dennis M. Rodgers of the National Oceanic and Atmospheric Administration for their help in obtaining data and information used in this project; to Michael Contino of The Pennsylvania State University Computation Center for his assistance in many of the numerical aspects of this study; and to Nancy Warner and Delores Corman for skillfully preparing the manuscript.

This project was conducted under the sponsorship of National Science Foundation Grant ATM-8218208, USAF AFOSR-83-0064, and NOAA Cooperative Agreement NA82AA-H-00027.

REFERENCES

Bartels, D. L., and A. A. Rockwood, 1983: Internal structure and evolution of a dual mesoscale convective complex. *Preprints, 5th Conf. on Hydrometeorology,* Tulsa, Amer. Meteor. Soc., 97–102.

Bosart, L. F., and F. Sanders, 1981: The Johnstown flood of July 1977: A long-lived convective system. *J. Atmos. Sci.,* **38,** 1616–1642.

Cahir, J. J., J. M. Norman and D. A. Lowry, 1981: Use of a real time computer graphics system in analysis and forecasting. *Mon. Wea. Rev.,* **109,** 485–500.

Fritsch, J. M., and J. M. Brown, 1982: On the generation of convectively driven mesohighs aloft. *Mon. Wea. Rev.,* **110,** 1554–1563.

——, R. J. Kane and C. R. Chelius, 1986: The contribution of mesoscale convective weather systems to the warm season precipitation in the United States. *J. Climate Appl. Meteor.,* **25,** 1333–1345.

Howard, K. W., and R. A. Maddox, 1983: Precipitation characteristics of two mesoscale convective systems. *Preprints, 5th Conf. on Hydrometeorology,* Tulsa, Amer. Meteor. Soc.

Hoxit, L. R., R. A. Maddox, C. F. Chappell, F. L. Zuckerberg, H. M. Mogil, I. Jones, O. R. Greene, R. E. Saffle and R. A. Scofield, 1978: Meteorological analysis of the Johnstown, Pennsylvania flash flood, 19–20 July 1977. NOAA Tech. Rep. ERL 401-APCL43, 71 pp.

Kane, R. J., 1985: The temporal and spatial characteristics of precipitation from mesoscale convective weather systems. M.S. Thesis, Department of Meteorology, The Pennsylvania State University, 152 pp.

Kincer, J. B., 1916: Daytime and nighttime precipitation and their economic significance. *Mon. Wea. Rev.,* **44,** 628–633.

Leary, C. A., and E. N. Rappaport, 1987: The life cycle and internal structure of a mesoscale convective complex. Accepted by *Mon. Wea. Rev.*

Maddox, R. A., 1980: Mesoscale convective complexes. *Bull. Amer. Meteor. Soc.,* **61,** 1374–1387.

——, 1983: Large-scale meteorological conditions associated with midlatitude mesoscale convective complexes. *Mon. Wea. Rev.,* **111,** 1475–1493.

——, C. F. Chappell and L. R. Hoxit, 1979: Synoptic and mesoscale aspects of flash flood events. *Bull. Amer. Meteor. Soc.,* **60,** 115–123.

——, D. J. Perkey and J. M. Fritsch, 1981: Evolution of upper tropospheric features during the development of a mesoscale convective complex. *J. Atmos. Sci.,* **38,** 1664–1674.

——, D. M. Rodgers and K. W. Howard, 1982: Mesoscale complexes over the United States during 1981—annual summary. *Mon. Wea. Rev.,* **110,** 1501–1514.

McAnelly, R. L., and W. R. Cotton, 1986: Meso-β scale characteristics of an episode of meso-α scale convective complexes. *Mon. Wea. Rev.,* **114,** 1740–1770.

McCann, D. W., 1983: Synoptic patterns associated with splitting thunderstorms. *Preprints, 13th Conf. on Severe Local Storms.* Tulsa, Amer. Meteor. Soc., J1–J4.

Merritt, J. H., 1985: The synoptic environment and movement of mesoscale convective complexes over the United States. M.S. Thesis, Department of Meteorology, The Pennsylvania State University, 129 pp.

——, and J. M. Fritsch, 1984: On the movement of the heavy precipitation areas of midlatitude mesoscale convective complexes. *Preprints, 10th Conf. on Weather Forecasting and Analysis,* Tampa, Amer. Meteor. Soc., 529–536.

Orlanski, I., 1975: A rational subdivision of scales for atmospheric processes. *Bull. Amer. Meteor. Soc.,* **56,** 527–530.

Pani, E. A., and D. R. Haragan, 1981: A comparison of Texas and Illinois temporal rainfall distribution. *Preprints, 4th Conf. on Hydrometeorology,* Reno, Amer. Meteor. Soc., 76–80.

Rodgers, D. M., K. W. Howard and E. C. Johnston, 1983: Mesoscale convective complexes over the United States during 1982—annual summary. *Mon. Wea. Rev.,* **111,** 2363–2369.

——, M. J. Magnano and J. H. Arns, 1985: Mesoscale convective complexes over the United States during 1983. *Mon. Wea. Rev.,* **113,** 888– 901.

Smull, B. F., and R. A. Houze, Jr., 1985: A midlatitude squall line with a trailing region of stratiform rain: Radar and satellite observations. *Mon. Wea. Rev.,* **113,** 117–133.

Wetzel, P. J., W. R. Cotton and R. L. McAnnelly, 1983: A long-lived mesoscale convective complex. Part II: Evolution and structure of the mature complex. *Mon. Wea. Rev.,* **111,** 1919–1937.